

On-site Determination of Corrosion rate under Stress of the of AZ31-B Magnesium Alloys Modified by the Friction-Stirring Process

W. Aperador*, J. Cortes, A. Delgado

Department of Engineering, Universidad Militar Nueva Granada, Carrera 11 No. 101-80, Fax:+57(1) 6343200, Bogotá, Colombia.

*E-mail: g.ing.materiales@gmail.com

Received: 30 August 2013 / Accepted: 5 October 2013 / Published: 1 October 2013

We performed the construction of a equipment, which was adequate to a potentiostat galvanostat for the on-site evaluation of the corrosion under stress of the AZ31-B magnesium alloy modified by the friction-stirring process, with the purpose of determinate the effect of the applied stress and the degradation. Analyses were performed by electrochemical impedance spectroscopy and potentiodynamic polarization curves. It was observed that a welded alloy generates higher corrosion velocities which cause a lower corrosion resistance in saline environments, apparently related with the continuous cracks propagation by anodic dissolution.

Keywords: corrosion, stress, AZ31B magnesium, friction-stir.

1. INTRODUCTION

The corrosion under stress test are performed in different ways, for example a test is destined to find the corrosion type and the velocity rate on a specimen of AISI 304 steel in the presence of an aqueous medium (Na₂S₂O₃) [1]. The synergy of a mechanical test and electrochemical process can lead to crack propagation phenomena known as: intergranular or transgranular propagation. This test takes hours, and is performed by applying a stress and incrementing it every so often until the rupture of the specimen. [2] In this case, the specimen presents intergranular crack propagation [3-4].

Other test is oriented to characterize the corrosion under stress process, which by means of a slowly increasing of the stress on a 304 stainless steel specimen, is observed the increasing of the strain and deformation of the specimen as well as its behavior against the corrosion in an aqueous medium of NaCl [5-6]. Analyzing the corrosion products presented on the specimen in the whole

process of stress-strain, was observed that can be develop gradually from the localized corrosion to the general corrosion depending on the stress [7].

To determinate the Mg-Al (AZ91, AZ31 y AM30) alloys behavior in distilled water. Other test was proposed, performing corrosion under stress characterization by hydrogen cooling technique [9]. From these alloys was found that the more resistant in the test was the AM30 followed by the AZ31 (55-75 MPa, 105-170 MPa) where were presented a located corrosion; and the least resistance was the AZ91 (130-140 MPa), but was found a considerable higher damage in the AZ91 alloy [10].

In the industry, the materials are always subject to different types of stress; a mechanical element is designed, with the purpose that it works in the elastic zone of the material [11], to avoid permanent deformations of the material when is being used. The corrosion under stress tests are performed in-site, but with greater variations in comparison with the real environment. For example, the stress applied to the specimen is increased gradually [12], or is increased without an interest in what zone the corrosive process is applied [13], since the corrosive test is presented during the whole deformation.

The aim of this work is to show the development of equipment that identifies the stress-strain graphic and determine when the applied stress to the specimen is leading the material to the end of the elastic zone. At this point, the equipment stops the stress increases and the corrosive processes are applied, with this is guaranteed that the stress is the maximum allowable without suffer permanent deformations as well as the tests are performed at the elastic zone, as is presented in the industry.

2. EQUIPMENT DESCRIPTION

For the implementation of the corrosive process is used a electrochemical cell that allows to perform controlled chemical reactions in its interior without being affected or reacted with the aqueous medium in which the material is to be evaluated (figure 1).

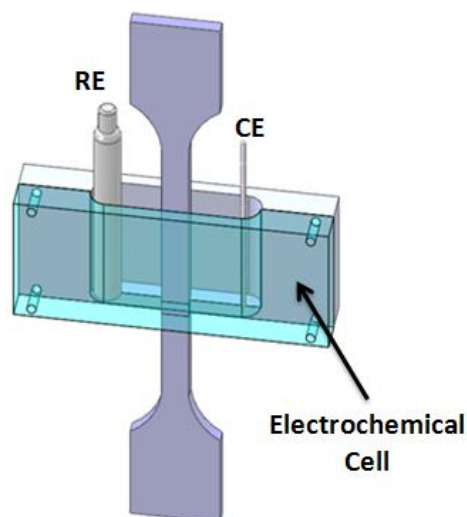


Figure 1. Electrochemical cell set.

On the basis of the shape, the specimen length (60 mm) and the evaluated area on the material; the size of the reference electrodes (ER, 6 mm of diameter by 80 mm of length) and counter electrode (CE, 1 mm of diameter by 80 mm of length) will be imposed design patterns for its correct implementation. Following the indications of the ASTM E8 standards and carry on the test to the peak yield strength, subsequently evaluate the corrosives processes by electrochemical impedance spectroscopy (EIS) and polarization curves techniques [14].

Fig 2 shows the connection between the electrochemical cell and the potentiostat galvanostat. The terminals that the equipment requests to connect are the reference electrode (RE), working electrode (WE) and the counter electrode (CE), which are the same as referenced in the electrochemical cell for its connection.

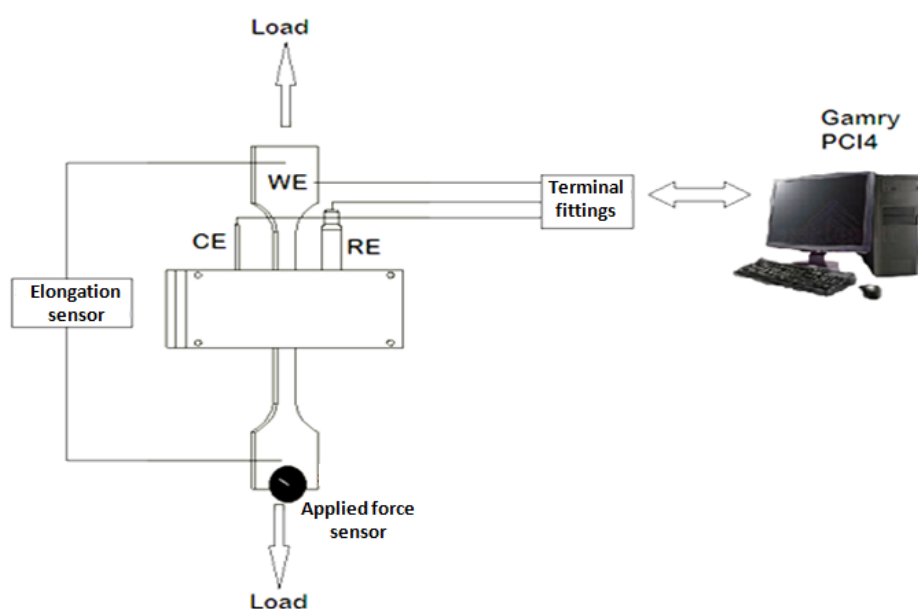


Figure 2. Electrochemical cell connected to the potentiostat galvanostat.

Figure 3 shows the coupling of the used systems to perform the corrosion under tension test. Performing the following procedure:

- Mounting of the specimen in the electrochemical cell: the mounting of the specimen within the electrochemical cell consists in put the specimen in a recipient (electrochemical cell) capable of storing an aqueous medium in the company of the specimen, and then the electrodes (see figure 1).
- Mounting in the universal testing machine: From having the electrochemical cell set, it should be placed in the machine to perform the corrosion under tension test and are coupled by subsection of the specimen with some mandrels.
- Provide the necessary data and run the software: Having the correct mounting in the machine, we proceed to provide the input information to the software (initial length and transversal area. (See figure 7) and the required displacement velocity relative (see figure 6). Then the software

is started, it begin to increase the force applied to the specimen and acquire step by step the data of the stress-strain behavior and corroborating each date to place in what point of the elastic zone is in order to find the stress point of the yield strength.

- Apply corrosion processes: after finding the point of the yield strength, the specimen is subjected to the corrosive processes, beginning with a non destructive test of electrochemical impedance spectroscopy (EIS) and Tafel polarization curves using a PCI4 Gamry Potentiostat Galvanostat while the software is acquired data of the stress variation in the specimen during the corrosive processes (see figure 3).

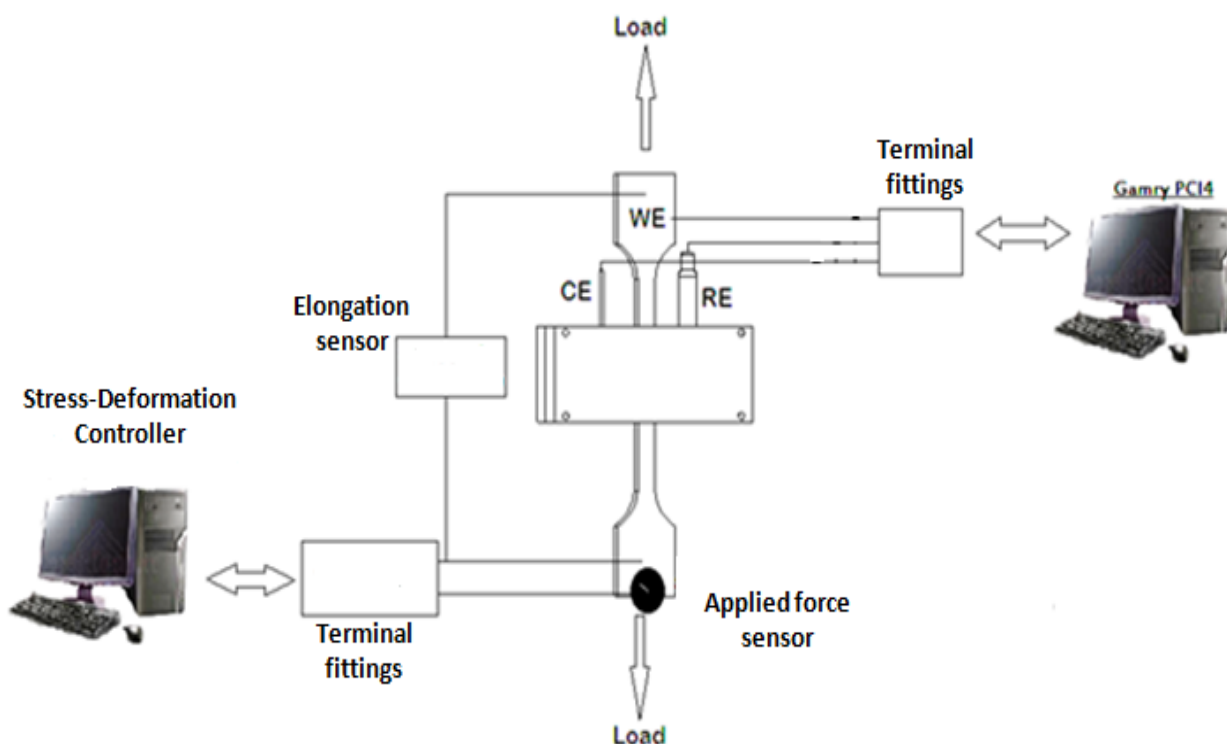


Figure 3. Complete set of the corrosion under tension test

2.1 Control Software

With the purpose of evaluate the method of corrosion under tension, described in the previous sections, was developed software that allows finding the stress-strain curve, which controls the point where the elastic zone ends and the displacement velocity relative of the applied force depending on the material. The software was programmed under the development platform NI LabView, which is an ideal environment for any measurement and control system, and a development environment to solve problems.

The applicative has divided screen in five zones (see figure 4):

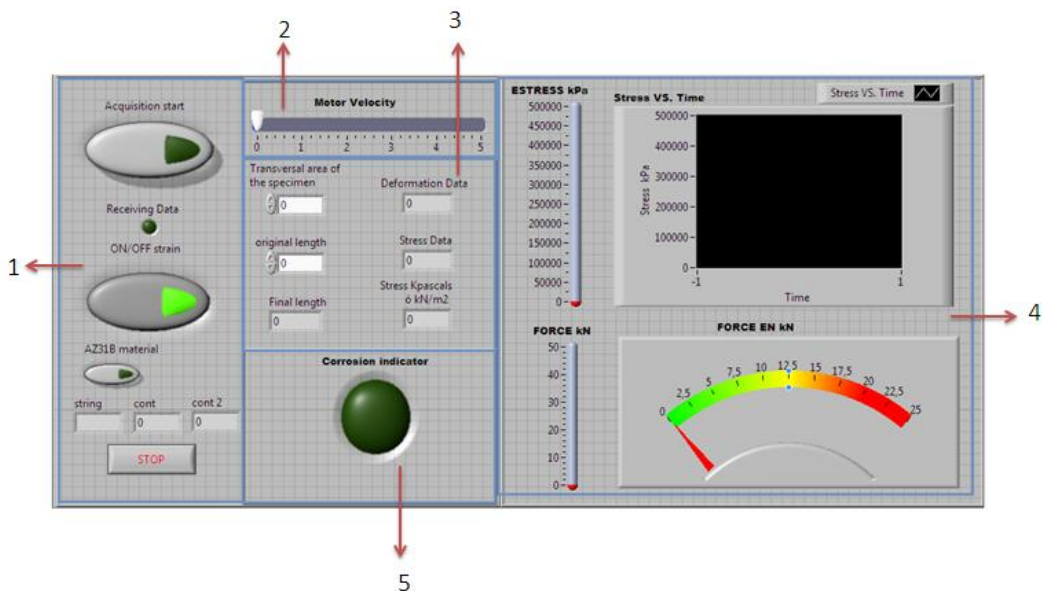


Figure 4. Graphic user interface Interfaz (GUI) of the control software (Distribution Zone)

1. *Control test status zone:* the control zone has three buttons (see figure 5), (a) Start button: to control initiation of the data acquisition from the stress sensor and the strain sensor. (b) Button force application: is charged of increase or stop the applied force to the specimen. (c) Stop button: button to end the test.

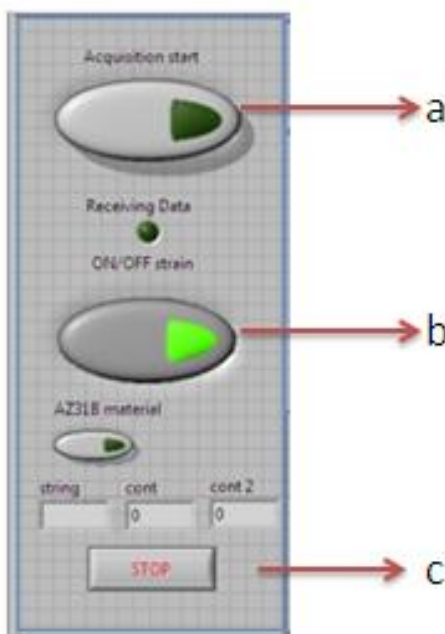


Figure 5. Control test zone

2. *Motor control zone:* The motor control zone has a slider bar which makes possible to control the motor velocity, also has an indicator where five indicates the maximum value of rpm (rpm) and zero indicates the minimum value (3 rpm) see figure 6.



Figure 6. Motor control zone

3. *Settings of the specimen zone:* This zone has six text fields in which are possible to set the specimen type that will be subjected to the test by typing the required parameters. (See figure 7).
 (a) Text field for input the specimen area: Field for typing the transversal area of the specimen.
 (b) Text field for input the specimen initial length: Field for typing the initial length of the specimen.
 (c) Final data input indicator: visualization string of the deformation.
 (d) Data for deformation graphic indicator: Deformation data to plot.
 (e) Data for stress graphic indicator: Stress data to plot.
 (f) Stress visualization: Data of the applied stress.

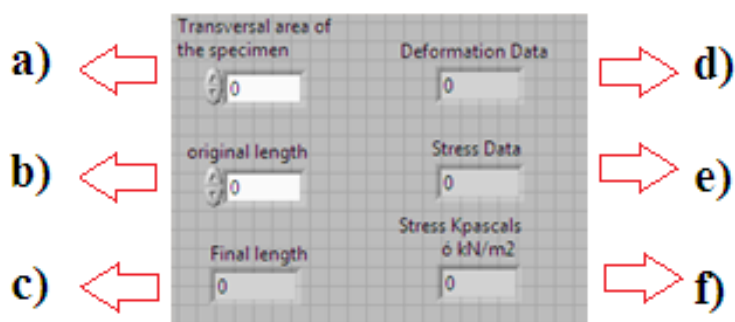


Figure 7. Settings of the specimen zone

4. *Corrosion control zone:* The corrosion control zone includes a pilot that indicates the moment in which is reached the point of the stress to yield strength with the purpose to start the corrosive action on the system (see figure 8).

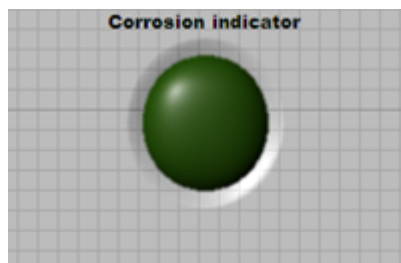


Figure 8. Motor control zone

5. *Visualization zone:* This zone presents two graphical fields that represent the strain on the specimen and the applied force (see figure 9).
 (a) Strain curve in the time: Shows the specimen behavior through the time.
 (b) Applied force indicator: Allow to visualize the applied force on the specimen.



Figure 9. Visualization zone

2.2 Evaluation techniques

For the evaluation of the corrosion resistance at static conditions was used a potentiostat – galvanostat Gamry PCI-4 model. Techniques of electrochemical impedance spectroscopy (EIS) and anodic polarization curves were used. The electrochemical corrosion tests were performed at a temperature of $25 \pm 0.2^\circ\text{C}$, using as electrolyte NaCl 0.5M. For mounting was used a cell composed by a counter electrode of platinum, a reference electrode of Ag/AgCl and as working electrode were used the AZ31B magnesium alloys, The specimens were cut to a length of 160 mm by 80 mm wide, for carrying out the welds. The friction stir process (FSW) was performed using a universal mill, equipped for a rotation speed of 1500rpm and welding speed of 136 mm / minute and keeping the penetration of 3 mm and inclination of the tool 1° . The chemical composition of the base material obtained by analysis of X ray fluorescence is shown in the table 1. The specimens to evaluate were polished previously, until obtain a low rugosity surface, which was achieved using abrasive paper of increasing size of SiC, from size of 100 to 1200, and finally polishing the specimens with alumina suspensions (Al_2O_3) of 1.0 and $0.05 \mu\text{m}$ on rotating disc. The Bode diagrams were obtained performing frequency sweeps in a range of 0.1 Hz to 100 kHz, using a sinusoidal signal amplitude of 10 mV. The polarization curves were measured after one hour of immersion, the current-potential curves were swept of 1 mV/s, in a range of voltages from $-0.25 \text{ V}_{\text{Ag/AgCl}}$ to $1.25 \text{ V}_{\text{Ag/AgCl}}$ with respect to the corrosion potential (E_{corr}). The values of corrosion rate (V_{corr}) were calculated from the Tafel slopes and the corrosion current density values (I_{corr}) in a potential range of $\pm 250 \text{ mV vs. } E_{\text{corr}}$, from the anodic polarization curves. Electrochemical tests were performed after the yield point, to find the value of stress corrosion cracking in situ [15].

Table 1. Chemical composition of the AZ31B magnesium alloy

Element	% in weighth
Al	3.0
Mn	0.20
Zn	0.9
Ca	0.04
Si	0.10
Cu	0.05
Ni	0.005
Fe	0.005
Mg	95.4
Others	0.30

3. RESULTS

3.1 Corrosion under tension test

The stress behavior of the specimen can be observe in the figure 10, which indicates that the acquired the maximum stress without exceed the elastic zone neither suffer permanent deformations of the material, this value was 78.235 MPa.

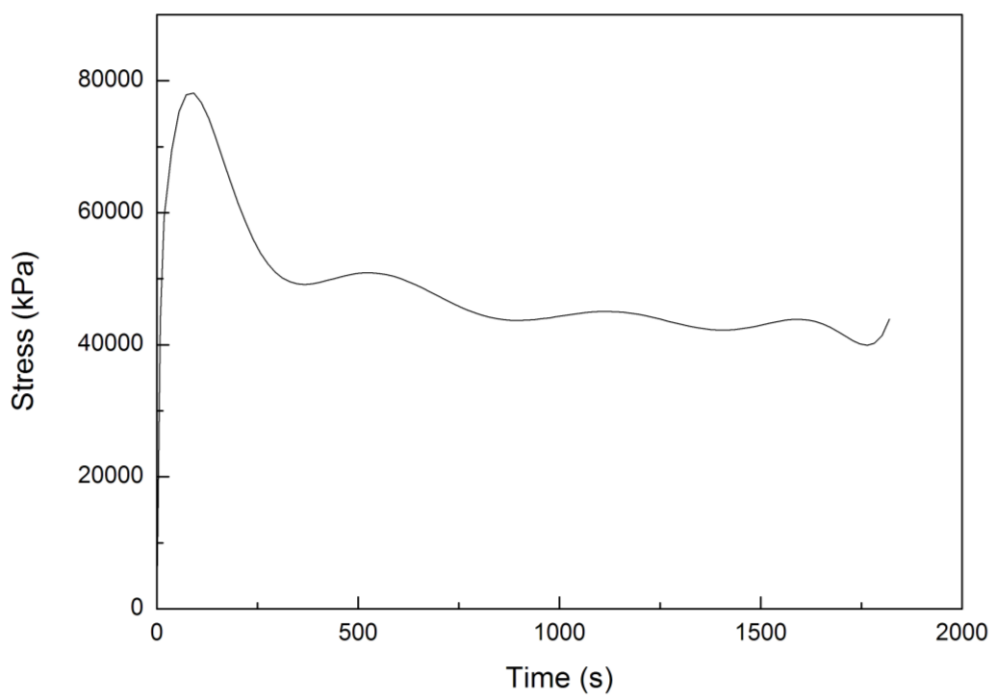


Figure 10. Strain in time.

3.2 Electrochemical evaluation

According to the anodic polarization curves shown in the figure 11, obtained in the potential intervals between $-0.25V_{Ag/AgCl}$ y $0.25 V_{Ag/AgCl}$, the corrosion potentials are moved to more noble values (protection), for the specimen which was not weld, and more active values for the welded specimens. It is due to the corrosion occurs firstly in superficial defects (as grain limits and dislocations) produced during welding, and oxide films and other passive films susceptible to nuclear in the crystalline defects, it generates the activation of the corrosion of the Mg phase, which is closely related to micro structural details [16].

During the welding process by friction is produced in the central zone a dynamic re-crystallization producing fine grains and equiaxed due to the influence of the process parameters in the micro-structure of the magnesium alloys welded by friction stir. Owing to this, the grain refinement and higher number of dislocations produces an increase in the corrosion in comparison with the specimen that it was not welded, therefore presents a better corrosion resistance.

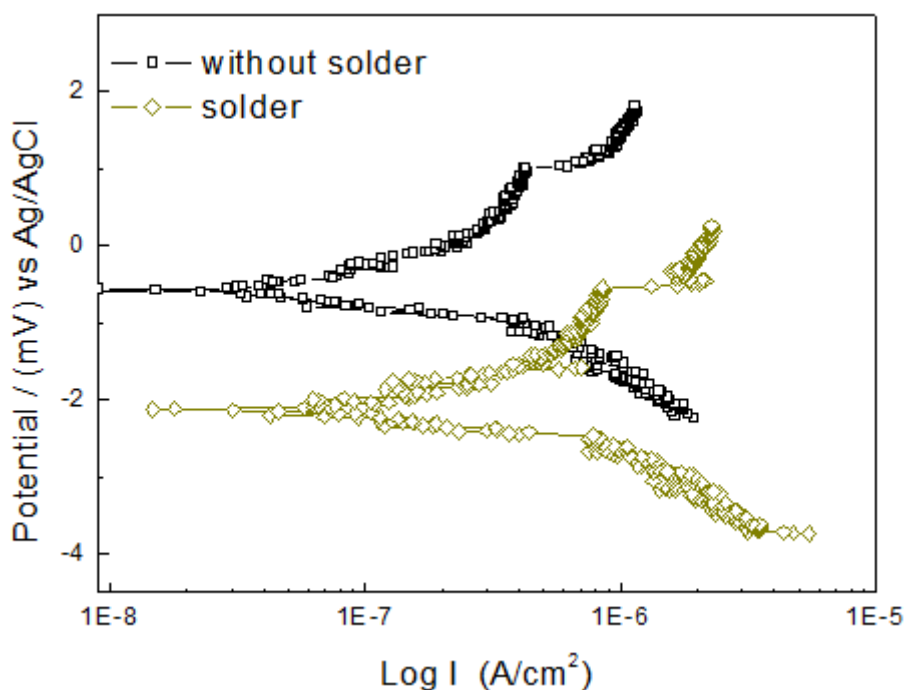


Figure 11. Tafel potentiodynamic curves of the magnesium alloy and the obtained weldings by the FSW process.

Comparing the values in the table 2, is seen that the FSW process presents a lower corrosion resistance, the density and corrosion rate values are dissimilar to that found for the material without welding, which present lower corrosion rate values generating a decrease in the corrosion density and velocity due to the microstructural change.

Table 2. Tafel potentiodynamic curves parameters of the magnesium alloy and the obtained weldings by the SFA process.

Specimen	Corrosion potential (mV)	Corrosion current (μA)	Corrosion rate (mpy)
Metal without soldering	-621	12	6.54
Metal solder	-2120	26	14.18

Calculating the current density of interchange, after the analysis of the experimentally obtained data (Table 2), it can be determined that the process is under anodic control, this indicates a slower reaction in the passing of the electron to the metal surface and of its metallic ion to the surface, moreover in this process the formed film on the magnesium surface, a hydroxide makes the process more complex, given this it can state that the welding process modifies the surface in a greater grade due to the process variables and it is clearly reflected in the results.

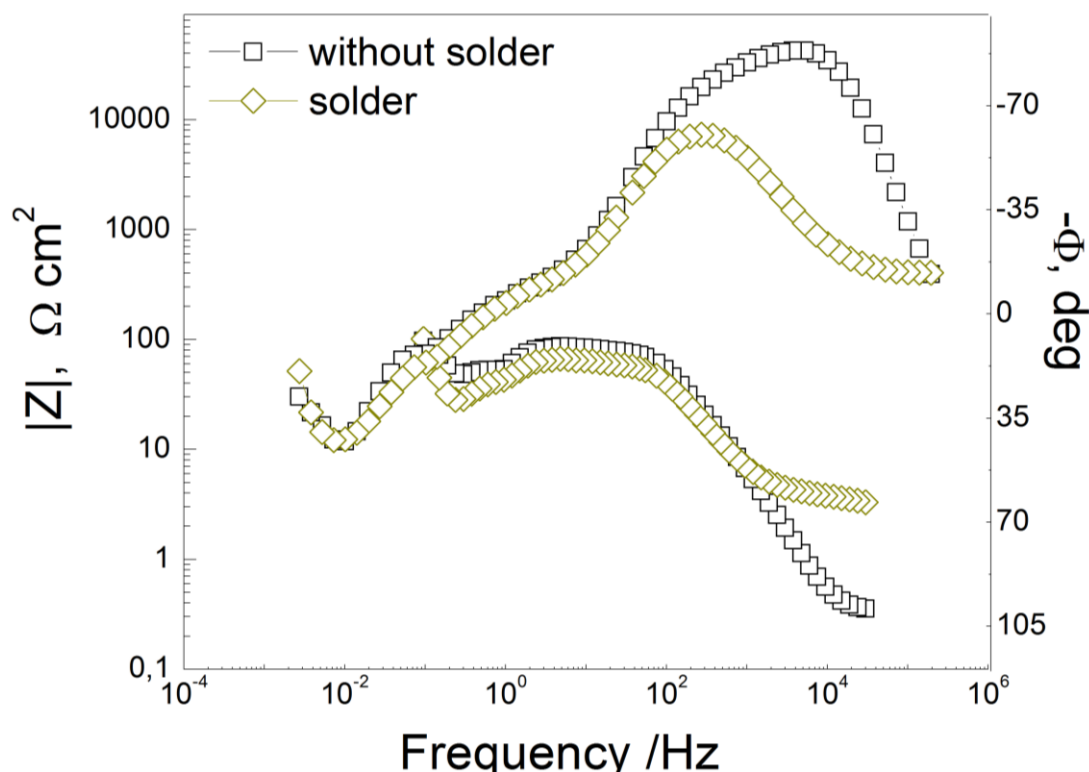


Figure 12. Bode diagram of the alloy.

The capacitive arc in the high frequencies can be related by the combination in parallel of the interphase capacitance and the resistance R1 (figure 13) of the charge transfer. In this case, the R1 is

used to evaluate the corrosion resistance of the specimens. The inductive curve at low frequencies can be attributed to partially protective films on the surface of the magnesium alloys.

In the figure 12 is shown the Bode diagram of the alloy without welding submerged in the NaCl solution at 0.5 M. In the diagrams is observed a capacitive behavior at high frequencies, in which is defined a flattened semicircle whose center is situated below the real axis (the center of the Nyquist diagram is rotated below the real axis with an angle ϕ). This phenomenon of semicircle flattening is associated with a process of dispersion in the frequency, due to the surface of the electrode is not homogeneous. Additionally, a diffusion process is observed, which pretends to define a second semicircle at low frequencies. The figure 4 also includes the results of the simulation using the electric circuit, indicated in the figure 5. As can be seen, there is a good concordance between experimental and simulated results. The magnesium alloy and the welding spectrum consist of a capacitive arc in the high frequencies range and an inductive arc in the low frequencies range.

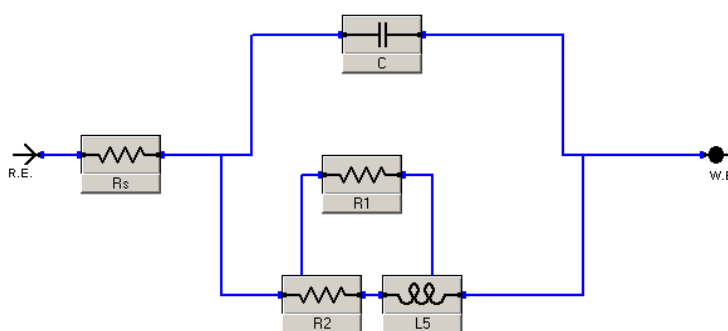


Figure 13. Equivalent circuit for stress corrosion testing.

In the figure 13, is observed the equivalent circuit of the AZ31B magnesium alloy (base material) and the obtained welding by the FSW process, where: C is the capacitance of the double layer and R_1 is the charge transfer resistance, when there are in parallel the response is characterized by the semicircle presence. The next step allows obtaining a simile of an electrochemical reaction that makes the analysis complex y the resistor in series to the parallel circuit RC , which represents the solution resistance, R_{sol} . This situation has the effect of transport the semicircle to greater values in the real impedance (Z') in the graphic, the R_2 resistance and the inductance L are associated to adsorption-desorption of specimens phenomena on the electrode surface, which alter the electrode potential and the corrosion rate of the metal [17].

4. CONCLUSIONS

The corrosion under stress for magnesium alloys is an extremely dangerous type of corrosion due to the continuous cracks propagation by anodic diffusion in the crack tip or discontinuous cracks propagation by a series of mechanical fractures in the tip of the crack. The anodic dissolution role is

produced by superficial defects that promote the hydrogen production which get into the material interior; the hydrogen can reduce the cohesive resistance of the magnesium alloys, resulting in hydrogen embrittlement. The monitoring of the corrosion under stress allows indicating by electrochemical techniques, that the corrosion under stress is more appreciable for welded materials using the FSW technique.

ACKNOWLEDGEMENTS

The authors acknowledge the at the Universidad Militar Nueva Granada

References

1. M.A. Mofid, A. Abdollah-zadeh, F. Malek Ghaini, *Mater. Des.*, 36, (2012) 161.
2. C. Shen, J. Zhang, J. Ge, *J. Environ. Sci.*, 23, (2011) S32.
3. A. Dhanapal, S. Rajendra, V. Balasubramanian, *Transactions of Nonferrous Metals Society of China*, 22 (2012) 793.
4. W. Aperador, G. Rodríguez, F. Franco, *Ingeniare. Rev. chil. ing.* 20 (2012) 119.
5. A. Scialpi, M. De Giorgi, L.A.C. De Filippis, R. Nobile, F.W. Panella, *Mater. Des.* 29 (2008) 928.
6. C. Liu, D.L. Chen, S. Bhole, X. Cao, M. Jahazi, *Mater. Charact.*, 60 (2009) 370.
7. A. Dhanapal, S. Rajendra Boopathy, V. Balasubramanian, *J. Alloys Compd.* 523 (2012) 49.
8. H.L. Hao, D.R. Ni, Z. Zhang, D. Wang, B.L. Xiao, Z.Y. Ma, *Mater. Charact.*, 52 (2013) 706.
9. M. Bobby Kannan, W. Dietzel, R. Zeng, R. Zettler, J.F. dos Santos, *Mater. Sci. Eng., A.* 460–461 (2007) 243.
10. M.A. Mofid, A. Abdollah-zadeh, F. Malek Ghaini, *Mater. Des.*, 36 (2012) 161.
11. P. Bala Srinivasan, R. Zettler, C. Blawert, W. Dietzel, *Mater. Charact.*, 60 (2009) 389.
12. Don-Hyun Choi, Byung-Wook Ahn, David J. Quesnel, Seung-Boo Jung, *Intermetallics.* 35 (2013) 120.
13. Masayuki Aonuma, Kazuhiro Nakata, *Mater. Sci. Eng., B.* 177 (2012) 543.
14. X. Cao, M. Jahazi, *Mater. Des.*, 30 (2009) 2033.
15. U.F.H.R. Suhuddin, S. Mironov, Y.S. Sato, H. Kokawa, C.-W. Lee, *Acta Mater.*, 57 (2009) 5406.
16. A. Razal Rose, K. Manisekar, V. Balasubramanian, *Transactions of Nonferrous Metals Society of China*, 21 (2011) 974.
17. W. Aperador, A. Delgado, F. Franco, *Int. J. Electrochem. Sci.*, 8 (2013) 9568 – 9577.